Animal models and high field imaging and spectroscopy

Gülin Öz, PhD; Ivan Tkáč, PhD; Kamil Uğurbil, PhD

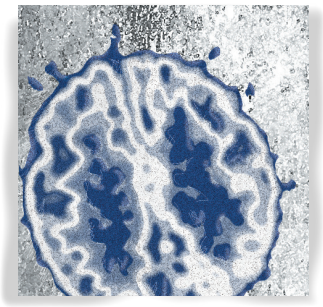

Introduction

In the last two decades, a plethora of magnetic resonance (MR) techniques have been introduced to provide indispensable measurement capabilities for studies of the brain in humans and in animal models of human diseased states. In addition to the exquisite anatomical information provided by MRI, these capabilities include imaging of brain function (functional MRI—fMRI), perfusion, vascular anatomy, diffusion, neurochemistry, and metabolic rates. At the same time, substantial gains in sensitivity and resolution with increasing magnetic field strength have been demonstrated (eg, ref 1) facilitating new discoveries as well as more robust preclinical and clinical applications of these techniques. Animal model

A plethora of magnetic resonance (MR) techniques developed in the last two decades provide unique and noninvasive measurement capabilities for studies of basic brain function and brain diseases in humans. Animal model experiments have been an indispensible part of this development. MR imaging and spectroscopy measurements have been employed in animal models, either by themselves or in combination with complementary and often invasive techniques, to enlighten us about the information content of such MR methods and/or verify observations made in the human brain. They have also been employed, with or independently of human efforts, to examine mechanisms underlying pathological developments in the brain, exploiting the wealth of animal models available for such studies. In this endeavor, the desire to push for ever-higher spatial and/or spectral resolution, better signal-to-noise ratio, and unique image contrast has inevitably led to the introduction of increasingly higher magnetic fields. As a result, today, animal model studies are starting to be conducted at magnetic fields ranging from ~11 to 17 Tesla, significantly enhancing the armamentarium of tools available for the probing brain function and brain pathologies.

Dialogues Clin Neurosci. 2013;15:263-278.

Keywords: *functional imaging; brain function; spectroscopy; neurometabolism*

Author affiliations: Center for Magnetic Resonance Research, University of Minnesota, Minneapolis, Minnesota, USA

Address for correspondence: Kamil Uğurbil, Center for Magnetic Resonance Research, University of Minnesota Medical School, 2021 Sixth street SE, Minneapolis, MN 55416, USA
(e-mail: kamil@cmrr.umn.edu)

Selected abbreviations and acronyms

MRI	*magnetic resonance imaging*
BOLD	*blood oxygen level-dependent*
CNR	*contrast to noise ratio*
MRS	*magnetic resonance spectroscopy*
NAA	*N-acetylaspartate*
GABA	*γ-aminobutyric acid*
AD	*Alzheimer's disease*
HD	*Huntington's disease*

studies have been an indispensible to these advances, particularly as part of efforts focused on increasing the magnetic field strength of human MR experiments. High field human studies started with the use of 4 Tesla (T) in 1991, when MR instruments employed in human imaging operated at 1.5 T or less. Ultimately, 7 T and, to a much lesser extent, to 9.4 T was established for human studies, largely justified by results obtained in animal model systems at such magnetic fields.[2]

Subsequent to the initial explorations of 4 T for human brain studies, a 9.4 T system was introduced for the first time for animal model experiments. This prototype instrument, with a bore large enough to perform studies in small- to medium-sized animals (eg, rodents and cats), provided the early forays (eg, refs 3-6) into the exploration of ultrahigh magnetic fields for functional, anatomical, and biochemical measurements in animal models using MR methods. Note that the terminology is based on classification of radiofrequency (RF) bands. The frequency range 300 MHz to 3 GHz is defined as ultra high frequency (UHF)—http://en.wikipedia.org/wiki/Ultra_high_frequency. The hydrogen nucleus resonance frequency at 7 T is ~300 MHz, ie, in the UHF band. Therefore, 7 to 70 T is defined as ultrahigh field (UHF). This body of work offered a clear demonstration of the advantages inherent at such fields and ultimately led to the development of instruments operating at even higher magnetic fields, such as 11.7, 14, 16.4, and 17 T. These ultrahigh field scanners provided significant and necessary new gains in resolution and sensitivity for animal model experiments.

High field MR imaging

Functional imaging

The effort to pursue high magnetic fields has been intricately tied to introduction of fMRI that can generate maps of human brain activity noninvasively. The very first fMRI experiments[7-10] were conducted at two different magnetic fields, 4 T and 1.5 T, providing the initial evidence that functional imaging may improve with increasing magnetic field strength; the results obtained at 4 T were at higher resolution and largely followed the contours of the gray matter ribbon, whereas the 1.5 T images of increased brain activity were more diffuse.[2] This field dependence was anticipated based on mathematical modeling[11] of the blood oxygenation level-dependent (BOLD) effect, which is based on the magnetic susceptibility difference between the intra- and extravascular space of deoxyhemoglobin containing blood vessels. This and other early (eg, refs 12-14) computational models of the BOLD phenomenon are currently understood to be largely accurate, albeit incomplete with respect to the mechanisms contributing to functional mapping signals. Some of these initially overlooked mechanisms (eg, inflow effects) form the basis of the successful use of lower field strengths, such as 1.5 T, for the acquisition of functional images in human brain. Nevertheless, increased understanding of the origin of fMRI signals (see ref 15 and references therein) have also reconfirmed original expectations that there are major advantages in going to very high magnetic fields, and these have largely been experimentally verified by a plethora of studies conducted with animal models (eg, refs 1, 16-18).

For example, in fMRI, the contrast-to-noise ratio (CNR) of deoxyhemoglobin-based BOLD mapping signals increases linearly in high-resolution imaging for gradient echo (GE)-based techniques, the predominant approach employed in contemporary fMRI experiments. (*Contrast* in fMRI is defined as the magnitude of the signal change induced by a stimulus or a task. *Contrast-to noise ratio* CNR is the ratio of the *contrast* to the signal fluctuations in the fMRI time series). When image resolution is high, the latter is dominated by the "thermal" noise present in each image of the time series. At low resolution, CNR for GE fMRI increases less than linearly with field magnitude since the temporal fluctuations of signals become dominated by physiological processes (rather than thermal noise) and display a dependence on signal amplitude, hence magnetic field magnitude. For spin echo (SE) BOLD fMRI, which provides more accurate functional localization,[1,16,17] albeit only at high magnetic fields and with smaller signal changes[1,9,20] CNR can exhibit more than a linear dependence on magnetic field magnitude because of supralinear gains in *fractional signal*

change induced by neuronal activity[19,20] and a linear elevation in intrinsic image signal-to-noise ratio (SNR).[21] The gains in fractional signal change, however, tend to level off at fields above ~9 to 10 Tesla,[15] leaving the SNR gains as the only potential source of CNR improvements.

More importantly, however, higher magnetic fields provide significantly better spatial fidelity in the deoxyhemoglobin-based functional mapping signals (eg, refs 1,16,17). fMRI relies on secondary metabolic and vascular responses invoked by alterations in neuronal activity. Therefore, its accuracy can be degraded by limitations imposed by these secondary responses. However, in a critical experiment performed in the cat visual cortex, it was demonstrated that blood flow increase induced by functional activation is regulated at the level of orientation columns. This observation indicated for the first time that cerebral blood flow (CBF) must be controlled at the capillary level, contradicting the accepted concept of the time that the "brain waters an entire garden for the sake of a single thirsty flower." Instead, these crucial animal model studies[22] suggested that the "brain waters specifically the thirsty flower, but also sprinkles the surrounding garden." The definitive conclusion of these cat visual cortex experiments was that the secondary physiological responses to neuronal activity would be compatible with very high-resolution functional mapping with CBF-based fMRI and potentially with BOLD based fMRI.

Compared with CBF methods, however, the BOLD approach suffers from additional confounds that can obfuscate spatial fidelity. They arise because blood vessels mediate the coupling between the physiological changes and the MR-detected functional signals; this coupling depends in a complex way on the diameter and oxygenation levels of the blood vessel involved (eg, refs 15,23,24). The consequences of these confounds were evaluated experimentally, most notably in animal models, but in humans as well. The point spread function (PSF) of the conventional GE fMRI was measured to be ~3.5 mm (full width at half maximum [FWHM])[25] at 1.5 T and ~2.5 mm at 4.7 T.[26] In contrast, the PSFs (FWHM) were reported as 1.64 ± 0.11 mm and 0.67 ± 0.08 for GE and SE fMRI, respectively, at 9.4 T in the cat visual cortex.[27,28] With a PSF of ~0.7 mm, columnar organization in 1 mm spatial scale and cortical laminar differentiations is easily possible without significant blurring. This has been demonstrated for several elementary organizations at the level of cortical layers[19,29-32] and cortical columns[30,33-39] in parallel studies conducted in the human brain and in the brain of animal model systems.[40-46] *Figure 1* illustrates an example from work examining laminar specificity in cat visual cortex using concurrent MR and histology studies.[44]

For animal model studies *only*, a highly desirable alternative to BOLD fMRI is cerebral blood volume (CBV)-based imaging using exogenous, intravascular contrast agents, typically superparamagnetic iron oxide particles, employed in high doses. This approach has been employed in studies ranging from rodents to the nonhuman primate (eg, refs 40,44,47-49), and was shown to have specificity to cortical layers and orientation columns.[40]

The magnetization of iron oxide agents saturate[47] at a relatively low magnetic field strength; as such, functional contrast arising from their presence does not increase significantly with increasing magnetic fields. Nevertheless, CNR for functional mapping has been reported to be about ~5[47] and ~3 times[49] higher with such agents compared with BOLD-based fMRI at low (1.5 – 2 T), and intermediate fields (3 - 4.7 T), respectively. It is possible that BOLD contrast will increase sufficiently at ultrahigh fields such as ~14 to 17 T so that it will in fact provide a preferable approach to iron oxide particles. However, neither these extremely high fields nor the use of these exogenous particles at such high doses are available for human brain studies. The former because such magnets with a large enough bore to accommodate humans remain beyond the scope of contemporary technology, and the latter because of potential toxicity concerns. Therefore, these technologies will remain applicable only to animal model studies for the foreseeable future.

To date, the vast majority of information accumulated about brain function is based on electrophysiological recordings of single- and multiple-unit activities in animal models, for example in instrumented, behaving nonhuman primates. Consequently, it was inevitable that the relationship between electrophysiological and fMRI data would be examined. Such experiments were naturally performed in animal models, continuing the trend of combining invasive but often more informative measurements with the noninvasive fMRI method. In simultaneously acquired data, the spiking activity and local field potentials recorded with implanted electrodes in the nonhuman primate were compared with BOLD

fMRI signal changes during visual stimulation,[50,51] indicating that local field potentials rather than spiking activity correlates with the BOLD fMRI signals. A similar strategy was employed in the cat visual cortex to examine the spatial relationship between single-unit activity and stimulus-induced fMRI maps obtained at 9.4 T.[52] When averaged over ~4x4 mm^2 cortical surface area, spiking activity and fMRI signals were found to be well correlated, but the correlation broke down progressively with diminishing surface area over which the averaging was performed. Especially at the level of individual electrode recording sites, the correlation between the two signals varied substantially because of the spatial inaccuracies inherent in GE BOLD fMRI.[52]

The electrophysiological recordings have also been employed to probe neuronal mechanisms underlying resting state fMRI (rfMRI) in animal models. (eg, refs 53-56). Unlike task- or stimulus-induced fMRI, rfMRI uses correlations in the spontaneous temporal fluctuations in an fMRI time series to deduce "functional connectivity"; it serves as an indirect but nonetheless invaluable indicator of gray-matter regions that interact strongly and, in many cases, are connected anatomically (eg, refs 57-62). Many of these studies reported a correlation between fluctuations in rfMRI signals and concurrent fluctuations in the underlying, neuronal activity measured locally with multiunit electrodes.

Such combined approaches continue to be used in animal models to probe numerous aspects of brain function, as well as the properties of functional imaging data; however, the literature in this field is too vast to cover comprehensively in this brief review.

Structural MRI

Structural MRI is increasingly accepted as a surrogate for anatomic phenotype in neuroscience research. In many areas, anatomic MRI has replaced the need for analysis of the postmortem brain in order to elucidate relationships between structure and function. It is not hard to find examples in which anatomic MRI has transformed the entire research landscape of a field: cerebrovascular disease, epilepsy, multiple sclerosis, and other inflammatory conditions, cerebral developmental disorders, to some extent psychiatric disorders, and neurodegenerative disorders. Animal model studies at high

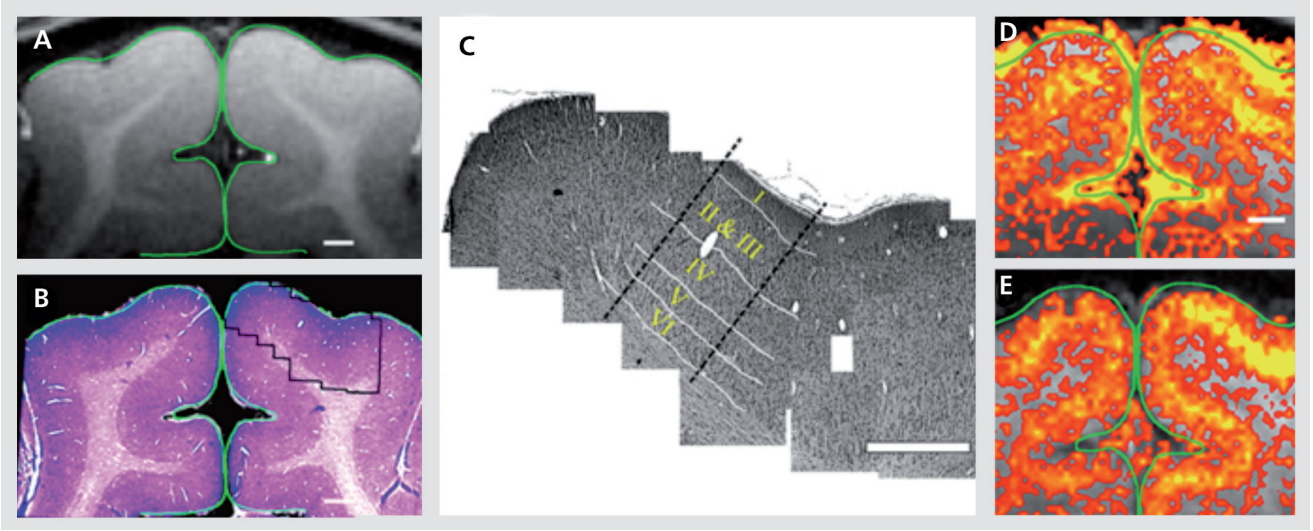

Figure 1. Coregistration of magnetic resonance (MR) image with the corresponding cortical tissue: Following the MR imaging session, the animals were sacrificed and the cortical tissue was stained for cytoarchitectonic structures. (a) A high-resolution MRI. (b) Low-magnification photograph of the corresponding Nissl stain (histology) of the same region. (c) A mosaic reconstruction of high magnified Nissl-stained images (right hemisphere) of cortical tissue corresponding to the imaged plane (outlined in panel b). White lines: the anatomically defined borders between cortical layers. (d) and (e) High-resolution blood oxygen level-dependent and cerebral blood volume functional MRI (0.15 x 0.15 mm^2) maps for a 40-s drifting bars stimuli. Signal changes were confined to the primary visual areas and closely followed the gray matter contour. In both maps, a spatially defined band of elevated signal changes was centered over layer IV as defined anatomically in panel c.
Adapted from ref 44: Harel N, Lin J, Moeller S, Ugurbil K, Yacoub E. Combined imaging-histological study of cortical laminar specificity of fMRI signals. *Neuroimage*. 2006;29:879-887.

magnetic fields have made unique contributions to this development.

Morphological images of brain tissue rely largely on proton density, T_1, and T_2 differences between tissue types (eg, white matter vs. gray matter, cortex vs. subcortical nuclei etc.). Proton density is clearly a magnetic field independent parameter. However, relaxation times T_1 and T_2 are field dependent, generally increasing[63,64] and decreasing[1,9,65,66] respectively, with higher magnetic fields (see review in ref 67). It was recently shown that, contrary to expectations, the dispersion in T_1 increases with increasing magnetic fields in the brain, leading to superior T_1-weighted structural images at the higher magnetic fields.[68]

Lengthening of T_1 with increasing magnetic field also holds true for blood. Blood T_1 is virtually insensitive to its oxygenation state. Ex vivo measurements have shown that blood T_1 varies linearly with field strength going from 1.5 T to 9.4 T according to $T_1 = 1.226 + 0.134B_0$.[69] This imparts a clear benefit in time-of-flight type vascular imaging, as well as perfusion imaging using spin labeling techniques. Mapping signals in all hemodynamic-based functional imaging methods, such as fMRI and optical imaging with intrinsic signals, are mediated through the vasculature. Consequently, vascular components in these methods are of utmost significance in determining the ultimate spatial and temporal accuracy of the neural activity maps produced by these methods. Therefore, it is important to be able to image vasculature in great detail, and ideally together with functional data in order to understand more precisely the source of the fMRI signals and their spatial correlation with the volume of altered neuronal activity. Vascular imaging with high resolution is also of paramount importance in other fields of biomedical research such as tumor biology, where angiogenesis is a necessary component of tumor growth.

Taking advantage of the gains in SNR and longer T_1 values, the feasibility of obtaining high-resolution MR images of intracortical vessels was demonstrated in the cat brain.[70] This accomplishment relied on a combination of time-of-flight MR angiography and T_2*-weighted contrast based on both endogenous BOLD effect and exogenous iron-oxide particles. It was possible to image vessels smaller than 100 microns, and distinguish between arteries and veins within the cortex[70] *(Figure 2)*.

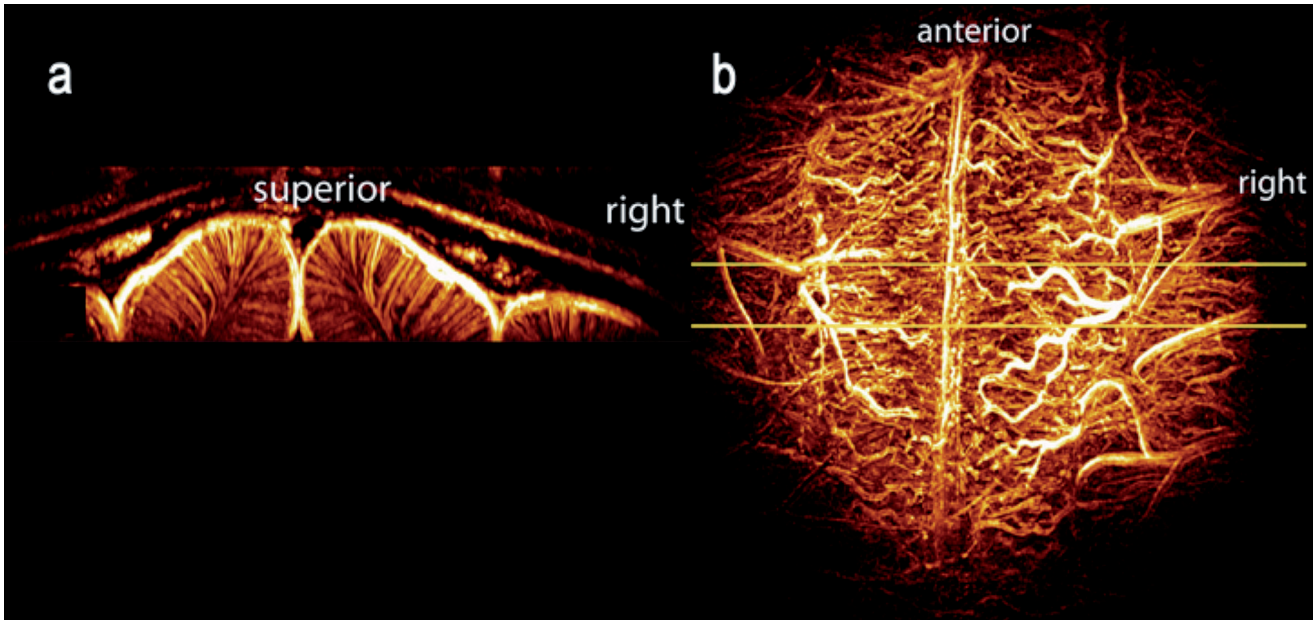

Figure 2. Maximum intensity Projections (MIPs) of the 3D vascular network in the cat, viewed in (a) coronal (left image) and (b) axial orientations. The axial projection (b) was performed over the full acquisition volume; the coronal projection (a) was produced from a narrow slab indicated by the yellow lines in (b). The coronal view clearly shows the uniform organization of intracortical vessels. The axial view is dominated by the vessels on the pial surface.
Adapted from ref 70: Bolan PJ, Yacoub E, Garwood M, Ugurbil K, Harel N. In vivo micro-MRI of intracortical neurovasculature. *NeuroImage*. 2006;32:62-69.

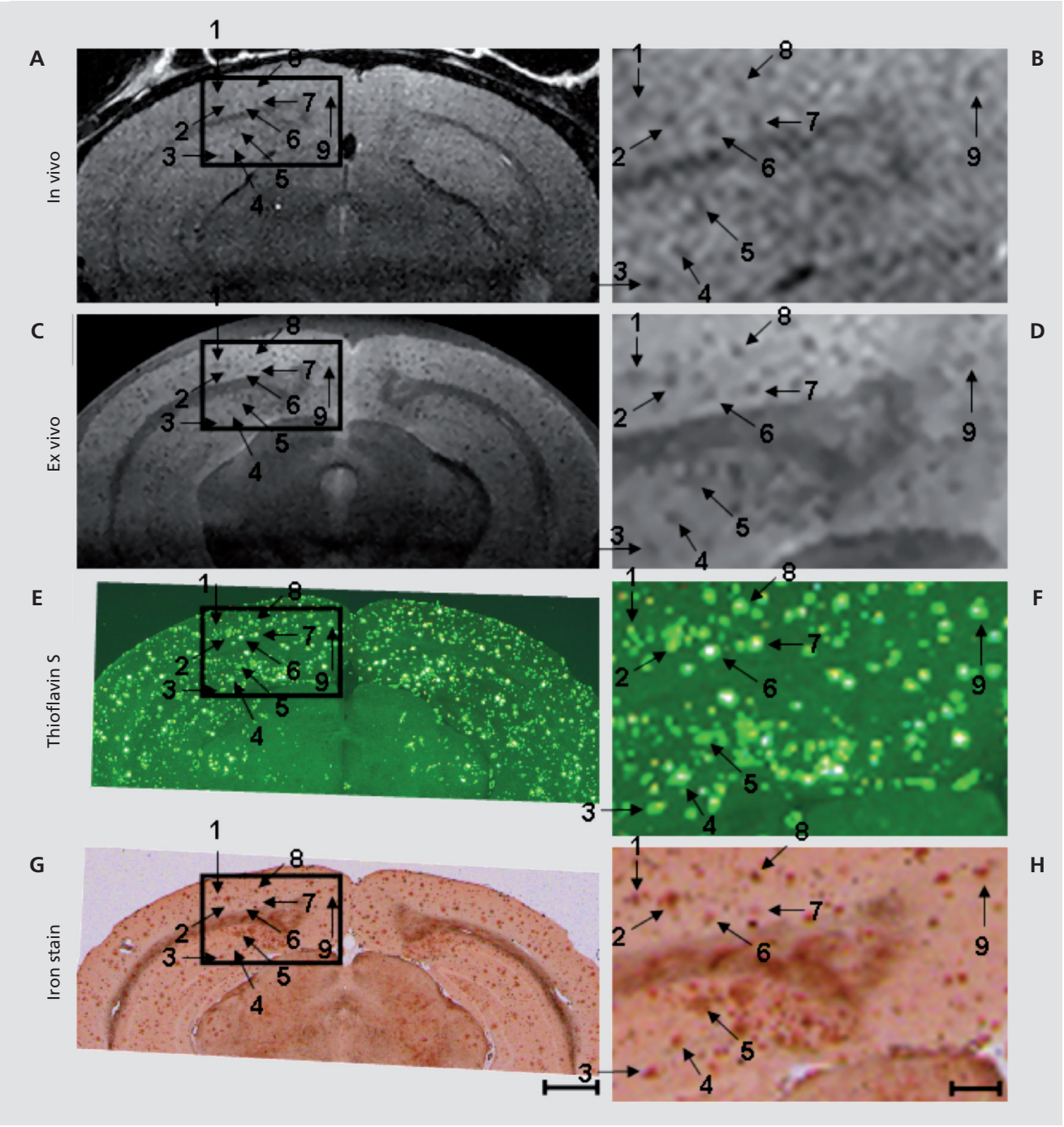

Figure 3. 9.4 T MRI and histology of 24 6-month 6-old AD mouse. In vivo MRI (A, B), ex vivo MRI (C, D), Thio-S (E, F), and iron stained images (G, H) have been precisely spatially registered over a circumscribed area of the cortex, indicated by the box. The boxes in the right column (scale bar = 100 μm) represent 3X magnified portions of the adjacent parent image in the left column (scale bar = 1.0 mm). Numbered arrows indicate individual plaques visualized in each of the four different image types.

Adapted from ref 79: Jack CR, Jr, Wengenack TM, Reyes DA, et al. In vivo magnetic resonance microimaging of individual amyloid plaques in Alzheimer's transgenic mice. *J Neurosci*. 2005;25:10041-10048. Copyright © Society for Neuroscience 2005

Such methods can be used for building models of the vascular network and may benefit a variety of research applications including fMRI, cerebrovascular disease, and cancer angiogenesis. Because of the lengthening T_1, and increased SNR, significant gains can be expected for such studies at even higher magnetic fields such as ~16 to 17 T.

At higher magnetic fields such as 14 to 17 T, other unique contrast mechanisms also come into play, leading to exquisite anatomical images obtained using approaches such as phase[71] and T_2*-weighted imaging, providing unprecedented visualization of anatomy in animal models.[72] The mechanism responsible for this improved anatomical imaging appears to be tissue-specific differences induced largely by myelin content and/or presence of iron.[73-77] Thus, the primary advantage of ultrahigh field for structural MRI is not just the SNR gain, which could be traded for increased spatial resolution at constant imaging times or imaging time at constant spatial resolution, but also gains in contrast mechanisms.

A recent and exciting example where the advantages of combined use of high magnetic fields and animal models were indispensable in morphological imaging has been the in vivo detection of amyloid plaques[78,79] *(Figure 3)* exploiting the genetic capabilities available in animal models. Among the neurodegenerative disorders, Alzheimer's disease has received much of the attention due to its frequency and hence high public health impact. Aβ plaques, a cardinal pathologic feature of Alzheimer's disease, were previously observed in T_2*-weighted images of ex vivo tissue specimens taken from the brain of AD mice. These plaques were imaged for the first time in vivo in anesthetized AD mice in reasonable imaging times (~1 hour)[78] using T_2 weighting at very high magnetic fields (9.4 T), incorporating strategies that minimize perturbations originating from breathing and brain pulsation. The mechanism responsible for this accomplishment is thought to be alterations in effective T_2 by diffusion-induced dynamic averaging of magnetic susceptibility gradients around the plaques. This contrast is small but depends quadratically on magnetic field magnitude. As such, the ultrahigh field was indispensable. Imaging of labeled plaques has been accomplished with other non-MR modalities (see references in ref 78). Unlike other modalities, however, MRI provides the potential for visualizing individual plaques non-invasively.

High field MR spectroscopy with protons

Neurochemical profiling in the animal brain

Proton (ie, ^{1}H) MRS, based on the proton resonance of hydrogen atoms, received considerable amount of attention in biomarker studies of neurological and psychiatric diseases[80] because it enables noninvasive detection of a number of endogenous small molecular weight neurochemicals directly in affected brain regions (eg, see detailed reviews in refs 81-83). Depending on the acquisition parameters, up to five neurochemicals can be quantified reliably from human brain at 1.5 T. Animal model studies at very high magnetic fields, where spectral resolution and sensitivity are enhanced, were critical in demonstrating the feasibility of going beyond this. Early studies employed animal brain tissue extracts at high-field MR instruments demonstrating the wealth of biochemical information available by MRS.[84-87] With recent advances in high-field MR instrumentation, spectroscopy localization techniques and sophisticated spectral quantification methods, however, the sensitivity and resolution of in vitro MRS was approached in the in vivo animal and human brain.[83]

Ten to fifteen neurochemicals in the human brain[88,89] and up to eighteen neurochemicals in the rat brain[90] can now be quantified noninvasively by high field MRS. In the mouse, which is highly desirable because of the availability of many models of human diseases, measurement of a 16-component neurochemical profile from 5-10 L volumes has been feasible.[91] The mouse brain studies encounter major challenges in MR instrumentation and methodology.[85,92] However, these difficulties were overcome in the last decade. The ability to measure an extended "neurochemical profile" increases the likelihood of identifying underlying processes on the molecular level, to detect disease-specific metabolic signatures and to directly assess mechanisms of drug actions, eg, by measuring endogenous antioxidant levels to assess effects of antioxidant medications.[93]

The technical and methodological challenges of MRS at high magnetic fields and the strategies to overcome them in order to fully benefit from increased sensitivity and chemical shift dispersion at high fields have been recently reviewed.[94] The quantification precision of MRS is improved at high fields,[89,95-97] which is critical for preclinical and clinical applications.

The most frequently studied MRS biomarker N-acetylaspartate (NAA) is localized almost exclusively to neurons and is used as a surrogate for neuronal cell number and viability.[98,99] Decreased NAA levels have been demonstrated in numerous neurological conditions and, therefore, are not very specific.[80] Neurotransmitters glutamate and γ-aminobutyric acid (GABA), which offer potentially more specific information about neuronal status, have also been reliably quantified in vivo with high field MRS. Glutamate is primarily localized to neurons,[100] with the highest levels present in excitatory terminals of glutamatergic neurons.[101] Decreased glutamate levels were observed in parallel with NAA in several neurological diseases and disease models,[85,102,103] likely because glutamatergic neurons make up the majority of neurons in the central nervous system (CNS). However, MRS detects both the neurotransmitter and metabolic pools of glutamate and alterations of glutamate levels in the absence of parallel NAA changes are possible.[86,104] Most inhibitory neurons in the CNS are GABAergic and have low levels of glutamate in their cell bodies and processes.[101] GABA is potentially a good marker for these neurons because GABA concentrations and GABA-like immunoreactivity are highest in these neurons.[105,106]

In addition to neuronal markers, MRS enables detection of several putative glial markers: cell culture studies suggested a primarily glial localization for myo-inositol[107] and its levels were increased with gliosis in the monkey and rat brain.[86,108] Therefore, increased myo-inositol levels have often been attributed to gliosis in neurological disorders.[102,109-111] However, the glial localization of myo-inositol has been disputed[112] and its levels do not always correlate with reactive astrogliosis.[113] Myo-inositol has multiple functions in cells. For example it plays an essential role in the regulation of cell volume in CNS as one of the most important organic osmolytes[112] and therefore may mark various cellular changes.

An alternative glial marker is glutamine, which can be reliably quantified using high field MRS. Glutamine is preferentially localized in glial cells,[100,101] and elevated glutamine levels were detected in diseases in which gliosis is known to occur.[102,109] Total creatine (creatine + phosphocreatine, tCr) and choline-containing compounds (tCho) are also highly concentrated in glial cells[114] and therefore may also increase with gliosis. Since both neurons and glia contain creatine and phosphocreatine, tCr has been utilized as a measure of total cellular density and its increase has been interpreted as glial proliferation that is not counterbalanced by neuroaxonal loss.[111,115] Choline-containing compounds, on the other hand, may also become increasingly MR visible with increased membrane turnover or breakdown, such as during active demyelination.[109,116] Therefore, tCr and tCho changes may have multiple implications that need to be determined for each disease in question.

In addition to the putative neuronal and glial markers, MRS can provide insights into energetic status and inflammation. For example, changes in the phosphocreatine-to-creatine ratio may be indicative of disturbances in energy metabolism.[117,118] Lactate increases can be associated with anaerobic metabolism of infiltrating macrophages or indicate impaired mitochondrial function.[109,116] MRS at high magnetic fields also allows the quantification of the most prominent antioxidants glutathione and vitamin C [88,89,119] and, thereby, can provide markers of oxidative stress.

MRS studies using animal models of human diseases facilitate biomarker identification and drug development because they allow delineation of the pathological correlates of biomarkers and screening of potential drugs in preclinical trials. As such, these animal studies enhance human applications of MRS, however, the interpretation and translation of animal data to human applications need additional considerations. First, the regional differences and developmental changes in metabolite levels[120] need to be taken into account when designing studies. Of note, the neurochemical profile of the rodent and human brain is very similar, with only few differences, such as very high taurine levels in the rodent brain *(Figure 4)*. Second, potential effects of anesthesia, which is necessary for animal scanning, need to be considered. General anesthesia was not found to affect steady-state levels of MRS detectable metabolites in the brain, except for glucose and lactate.[121,122]

Diagnosis

MRS can be utilized in preclinical and eventually clinical applications to distinguish, for example, transgenic mouse models from wild-type (WT) animals or patients from healthy controls. For the successful translation of biomarker data from animal models to humans,[123] not only does the model need to faithfully reproduce the pathology and phenotype of the human disease, but the same biomarker alterations need to be observed in the mouse model and in patients. This is a critical consider-

ation. MRS studies with various AD mouse models demonstrate this issue well. For example, among the different AD models studied with ^{1}H MRS, APP-PS1 mice match the neurochemical profile found in human AD best.[103] These mice display reductions in NAA and glutamate, as well as an increase in myo-inositol. The myo-inositol difference in particular had not been detected in other AD models, but is a prominent neurochemical alteration detected in human AD.[110] A more recent study demonstrated these neurochemical profile changes at an even earlier age than the APP-PS1 mice in a different AD mouse model.[124]

In MPTP-intoxicated mice, well-accepted model of the dopaminergic denervation in Parkinson's disease (PD), high field MRS enabled detection of elevated glutamate, glutamine and GABA levels in the striatum.[125] Of these alterations, the GABA difference was confirmed in human PD at ultra-high field.[126]

Longitudinal changes in neurochemical profiles were also reported in transgenic[117] and knock-in[118,127] mouse models of Huntington's disease (HD). The observed neurochemical changes varied between different mouse models[128] and relative to exploratory observations in human HD at 7 T,[129,130] which underlines the need for development of HD mouse models that fully mimic the phenotype and pathology of human HD.

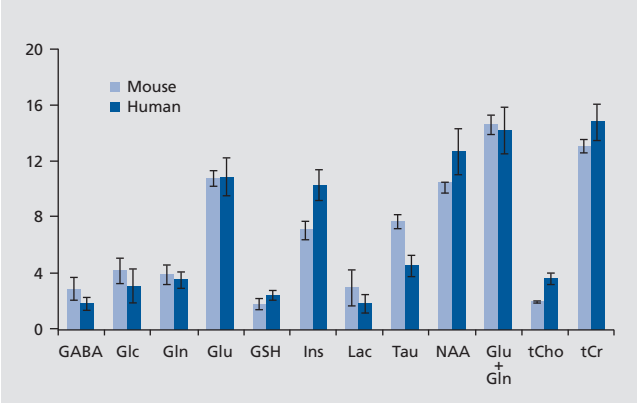

Figure 4. Neurochemical profiles of human and mouse cerebellum. Concentrations ± SD (μmol/g) obtained from the cerebellum of 16 healthy volunteers (35±15 years old) and 6 mice (C57BL/6, 6-8 weeks old) at 4T and 9.4T, respectively. The concentrations in the mouse brain were taken from Tkáč et al.[91] The same pulse sequence (STEAM) was used for mouse and human data with the following parameters: echo time TE =5 ms at 4T, 2 ms at 9.4T; repetition time TR =4.5 s at 4T, 5 s at 9.4T; voxel size 6.2 mL at 4T, 6.1 μL at 9.4T. GABA, γ-aminobutyric acid; Glc, glucose; Gln, glutamine; Glu, glutamate; GSH, glutathione; Ins, myo-inositol; Lac, lactate; Tau, taurine; NAA, N-acetylaspartate; tCho, total choline; tCr, total creatine

Adapted from ref 160: Oz G. MR Spectroscopy in health and disease. In: Manto M, Gruol DL, Schmahmann JD, Koibuchi N, Rossi F, eds. *Handbook of the Cerebellum and Cerebellar Disorders*. Vol 1. New York, NY: Springer Dordrecht; 2013:713-733. Copyright © Springer Dordrecht 2013

While conventional structural MRI detects neuronal loss and atrophy, ^{1}H MRS can be utilized to assess neuronal dysfunction, ie, it can reveal biochemical changes that may start years before symptoms and irreversible neuron loss in neurological diseases,[131] thereby facilitating early diagnosis in these diseases. Recent work on a transgenic mouse model of spinocerebellar ataxia 1 (SCA1) clearly demonstrated this potential to detect early neurochemical alterations by MRS. The SCA1 model used in these studies reproduces the Purkinje cell pathology seen in patients and develops progressive ataxia similar to the human phenotype.[132] Importantly, the same neurochemical alterations were detected by MRS in this model[133] and patients with SCA1[134] *(Figure 5)*. Furthermore, these neurochemical alterations were already detectable in the presymptomatic disease stage and marked neuronal dysfunction and dendritic atrophy, rather than cell loss, as shown by correlative histopathology.[133] These data indicate that MRS at very high magnetic fields may have a role in early diagnosis of neurological diseases in the clinic.

Monitoring of disease progression

MRS has been widely utilized for noninvasive monitoring of neurochemical alterations associated with disease progression in animal models and increasingly at high and ultra-high fields. For example, MRS was successfully applied in longitudinal studies of mouse models of various neurodegenerative diseases.[103,117,118,124,127,128,133] These studies demonstrated that changes in multiple neurochemicals associated with neurodegeneration, compromised neurotransmission, energy production, and osmotic regulation, can be monitored with high sensitivity using MRS in affected brain regions. In addition, such neurochemical changes correlate with semi-quantitative measures of pathological burden,[133,135] but precede tissue atrophy,[117,133] as well as clear behavioral symptoms.[133] In a SCA1 study, remarkably, the same neurochemicals (NAA, myo-inositol, and glutamate) correlated with the ataxia score in patients[134] and with the pathology scores in the mouse model,[133] indicating these metabolites as biomarkers of disease progression and substantiating an ability to translate the mouse findings to patients.

Monitoring of treatment and medication effects

Due to the ability to monitor neurochemistry longitudinally and noninvasively, MRS can also be used to monitor disease-modifying effects of treatments directly in affected brain regions and has been utilized in a number of preclinical disease and treatment models. Motivated by prior work that suggested nonsteroidal anti-inflammatory drugs (NSAIDs) may affect the incidence and progression of AD, the effects of chronic NSAID treatment was studied in a transgenic AD mouse model.[135] A significant protection against NAA and glutamate loss was demonstrated, suggesting that NSAIDs can protect against the neuronal pathology in AD. Similarly, dopamine administration, which had been the first-line pharmacologic treatment for PD for many years, reversed the abnormal striatal neurochemical levels (glutamate, glutamine, and GABA) in a PD model to WT levels.[125] In a SCA1 model, conditional expression of the transgene was utilized to establish the sensitivity of MRS biomarkers to disease reversal.[136] Namely, doxycycline treatment to suppress transgene expression was

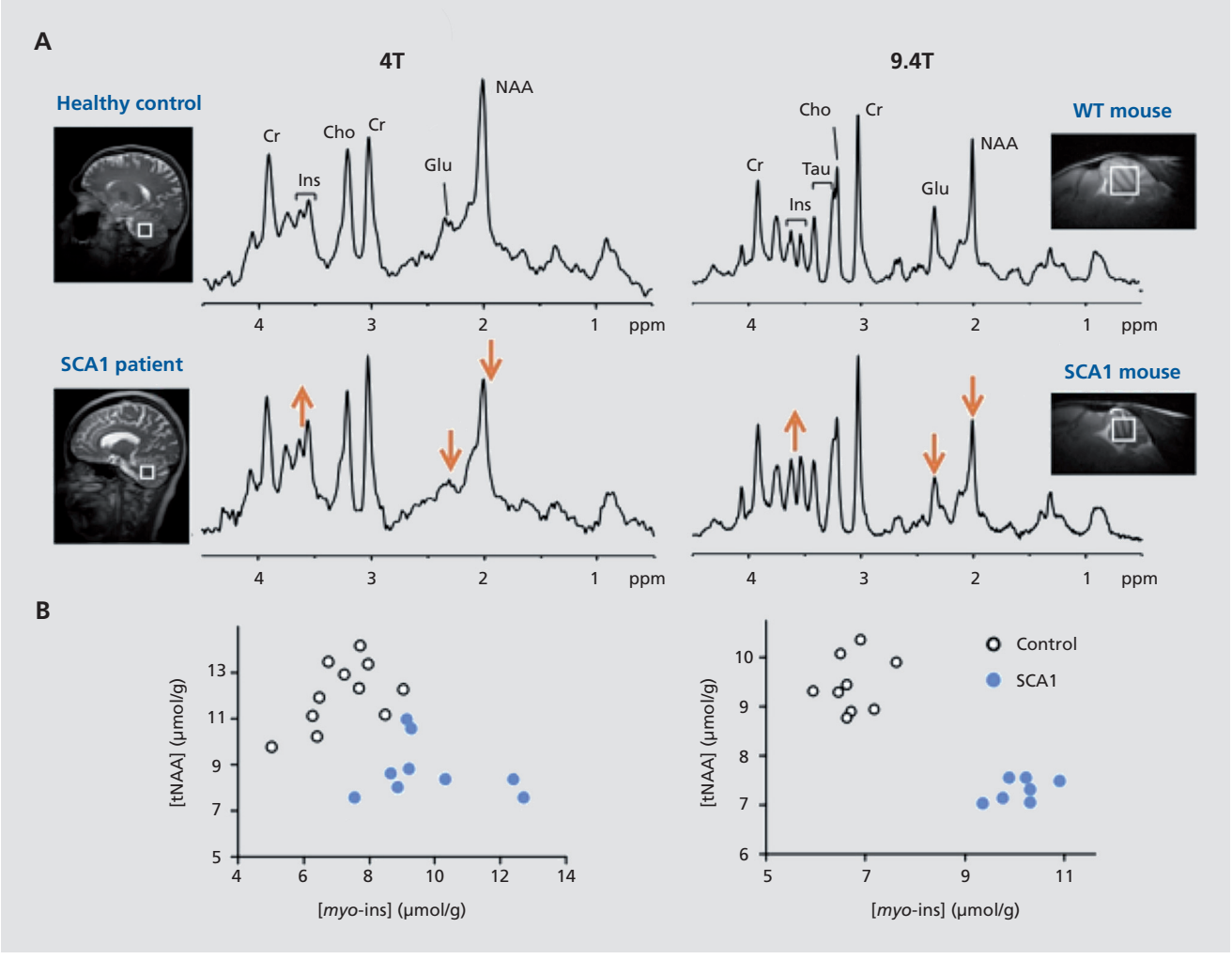

Figure 5. Parallel neurochemical alterations in patients[134] (left) and transgenic wild-type (WT) mouse models[133] of neurodegeneration (right). (A) Single-voxel ^{1}H MR spectra obtained from the cerebellum of a patient with spinocerebellar ataxia type 1 (SCA1) and a mouse with the same genetic mutation are shown in comparison to their respective healthy controls. Total N-acetylaspartate (NAA) and glutamate are lower and myo-inositol higher than controls in both cases. (B) Concentrations of NAA and myo-inositol obtained from individual subjects distinguish the SCA1 and control groups with no overlap in both humans and the mouse model.

shown to reverse the abnormal neurochemical concentrations towards control levels.[136] Furthermore, the potential to monitor treatment effects in individual mice by utilizing multiple neurochemical levels at once was demonstrated in this study.

In addition to longitudinal studies with chronic treatments, MRS can be utilized to monitor acute effects of drugs by obtaining time courses of metabolite levels. For example, neurochemical changes, including transient ones, upon acute phencyclidine (PCP) administration were captured in the rat brain, suggesting that MRS can be used to assess the effects of potential antipsychotic drugs in vivo.[137] Similarly, the effects of the antiepileptic drug vigabatrin on GABA levels were investigated in rat models using MRS,[138] and increases similar to those observed in the human brain[139] were detected.

Low gyromagnetic ratio nuclei

High field capabilities in brain research apply particularly to methodologies based on low gyromagnetic ratio nuclei such as ^{17}O and ^{23}Na imaging, and ^{13}C, and ^{31}P spectroscopy. For lower gyromagnetic nuclei, SNR gains provided by high magnetic fields can be more dramatic than what can be obtained for ^{1}H in large biological samples such as the human brain. For example, the SNR for the ^{17}O nucleus is elevated ~4 fold in conducting biological samples, including the rat brain, with magnetic field in going from 4.7 T to 9.4 T[140] while relaxation rates do not change. The SNR gain is within experimental error of expected theoretical maximum of 3.4[141] for these low frequencies since sample noise does not dominate SNR at these frequencies even in conducting samples.

The biological information content in MR studies conducted with such low gyromagnetic nuclei can be unique. For example, the ability to image and quantitatively measure $CMRO_2$ in the rat[140,142-144] and cat[145] was demonstrated and used to measure oxygen consumption changes associated with neuronal activity to obtain functional images using ^{17}O MR *(Figure 6)*. Similarly, ^{13}C and ^{31}P experiments have demonstrated the feasibility of measuring glutamatergic neurotransmission rates,[5,146,147] cerebral glycogen turnover,[148-152] glucose transport kinetics,[17,153-156] oxidative ATP synthesis rate,[157] and metabolic alterations in disease states.[158,159]

Conclusion

Animal model studies have played a critical role in evaluating the potential of the MR imaging and spectroscopy techniques to study basic brain function, brain diseases, and mechanisms underlying neuroimaging. Very high magnetic fields have been indispensable for achieving important gains in biological information content in these studies. The introduction of latest generation of MR systems operating at magnetic fields ranging from ~11 to 17 Tesla is expected to advance the field further for animal model experiments. ❑

Acknowledgments: The preparation of this review was in part supported by the National Institute of Neurological Disorders and Stroke (NINDS) grant R01 NS070815 (GÖ). The Center for MR Research is supported by National Center for Research Resources (NCRR) biotechnology research resource grant P41 RR008079, National Institute of Biomedical Imaging and Bioengineering (NIBIB) grant P41 EB015894 and NINDS grant P30 NS076408.

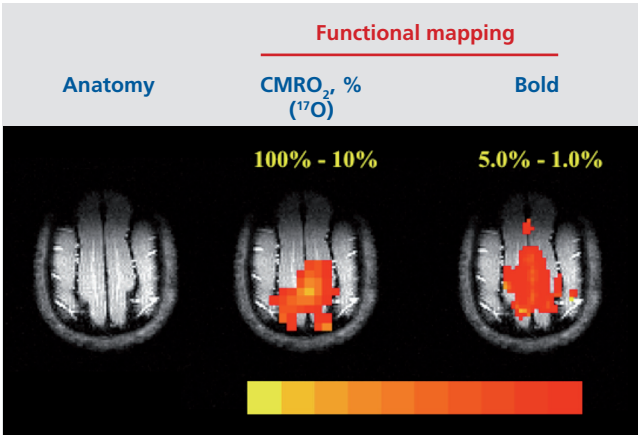

Figure 6. Functional imaging using ^{17}O to map % change in cerebral metabolic rate for oxygen ($CMRO_2$) vs blood oxygen level-dependent (BOLD) in the cat brain.
Adapted rom ref 145: Zhu XH, Zhang N, Zhang Y, Ugurbil K, Chen W. New insights into central roles of cerebral oxygen metabolism in the resting and stimulus-evoked brain. *J Cereb Blood Flow Metab*. 2009;29:10-18. Copyright © Raven Press 2009

Modelos animales y espectroscopía e imaginología de alto campo

Durante las dos últimas décadas se ha desarrollado una gran cantidad de técnicas de resonancia magnética (RM) que ha facilitado la posibilidad de mediciones especiales y no invasoras en los estudios de función cerebral básica y enfermedades cerebrales en humanos. Los experimentos en modelos animales han sido parte fundamental de este desarrollo. En modelos animales se han empleado imágenes de RM y mediciones de espectroscopía, tanto en forma aislada como en combinación con técnicas complementarias y con frecuencia invasoras, para darnos luces acerca del contenido de la información de los métodos de RM y/o verificar las observaciones realizadas en el cerebro humano. Estos procedimientos también se han utilizado, en conjunto o independientemente de los esfuerzos en humanos, para examinar los mecanismos subyacentes a los desarrollos patológicos del cerebro, explotando la riqueza de los modelos animales disponibles para tales estudios. En este intento, el deseo de impulsar cada vez mayores resoluciones espectrales y/o espaciales, una mejor relación señal/ruido y un contraste de imagen excelente ha llevado inevitablemente a la introducción de campos magnéticos cada vez más intensos. Como resultado de esto, hoy en día, los estudios de modelos animales están empezando a realizarse en campos magnéticos que van desde ~11 hasta 17 Tesla, lo que aumenta significativamente el arsenal de herramientas disponibles para evaluar la función cerebral y las patologías cerebrales.

Modèles animaux et imagerie et spectroscopie à champ élevé

Les techniques de résonance magnétique (RM) se sont incroyablement développées ces deux dernières décennies, permettant d'effectuer, de manière non invasive et originale, les mesures nécessaires à l'étude du fonctionnement cérébral humain normal et pathologique. Dans les modèles animaux expérimentaux indispensables à ce développement, les mesures par RM d'imagerie et de spectroscopie, seules ou en association à d'autres techniques complémentaires et souvent invasives, ont été utilisées pour nous éclairer sur leur fonctionnement propre et/ou vérifier les observations faites sur le cerveau humain. Elles ont également été employées, avec ou sans activité humaine, pour analyser les mécanismes sous-tendant les pathologies cérébrales grâce à la richesse des modèles animaux disponibles pour de telles études. Dans cette lancée, le désir d'obtenir une résolution spectrale ou spatiale toujours plus élevée, un meilleur rapport signal/bruit et une image de contraste originale, a inévitablement débouché sur des champs magnétiques de plus en plus élevés. Ainsi, aujourd'hui, les études de modèles animaux débutent à des champs magnétiques de 11 à 17 Tesla environ, ce qui enrichit significativement l'arsenal de moyens disponibles pour l'exploration de la fonction du cerveau et de ses pathologies.

REFERENCES

1. Ugurbil K, Adriany G, Andersen P, et al. Ultrahigh field magnetic resonance imaging and spectroscopy. *Magn Reson Imaging*. 2003;21:1263-1281.
2. Ugurbil K. The road to functional imaging and ultrahigh fields. *Neuroimage*. 2012;62:726-735.
3. Gruetter R, Weisdorf SA, Rajanayagan V, et al. Resolution improvements in in vivo 1H NMR spectra with increased magnetic field strength. *J Magn Reson*. 1998;135:260-264.
4. Lee SP, Silva AC, Ugurbil K, Kim SG. Diffusion-weighted spin-echo fMRI at 9.4 T: microvascular/tissue contribution to BOLD signal changes. *Magn Reson Med*. 1999;42:919-928.
5. Pfeuffer J, Tkac I, Choi IY, et al. Localized in vivo 1H NMR detection of neurotransmitter labeling in rat brain during infusion of [1-13C] D-glucose. *Magn Reson Med*. 1999;41:1077-1083.
6. Duong TQ, Kim DS, Ugurbil K, Kim SG. Spatiotemporal dynamics of the BOLD fMRI signals: toward mapping submillimeter cortical columns using the early negative response. *Magn Reson Med*. 2000;44:231-242.
7. Ugurbil K. Development of functional imaging in the human brain (fMRI); the University of Minnesota experience. *Neuroimage*. 2012;62:613-619.
8. Ogawa S, Tank DW, Menon R, et al. Intrinsic signal changes accompanying sensory stimulation: functional brain mapping with magnetic resonance imaging. *Proc Natl Acad Sci U S A*. 1992;89:5951-5955.
9. Kwong KK, Belliveau JW, Chesler DA, et al. Dynamic magnetic resonance imaging of human brain activity during primary sensory stimulation. *Proc Natl Acad Sci U S A*. 1992;89:5675-5679.
10. Bandettini PA, Wong EC, Hinks RS, Tikofsky RS, Hyde JS. Time course EPI of human brain function during task activation. *Magn Reson Med*. 1992;25:390-397.

11. Ogawa S, Menon RS, Tank DW, et al. Functional brain mapping by blood oxygenation level-dependent contrast magnetic resonance imaging. A comparison of signal characteristics with a biophysical model. *Biophys J*. 93;64:803-812.
12. Fujita N. Extravascular contribution of blood oxygenation level-dependent signal changes: a numerical analysis based on a vascular network model. *Magn Reson Med*. 2001;46:723-734.
13. Boxerman JL, Hamberg LM, Rosen BR, Weisskoff RM. MR contrast due to intravscular magnetic susceptiblity perturbations. *Magn Reson Med*. 1995;34:555-556.
14. Kennan RP, Zhong J, Gore JC. Intravascular susceptibility contrast mechanisms in tissue. *Magn Reson Med*. 1994;31:9-31.
15. Uludag K, Muller-Bierl B, Ugurbil K. An integrative model for neuronal activity-induced signal changes for gradient and spin echo functional imaging. *Neuroimage*. 2009;48:150-165.
16. Ugurbil K, Toth L, Kim DS. How accurate is magnetic resonance imaging of brain function? *Trends Neurosci*. 2003;26:108-114.
17. Ugurbil K, Adriany G, Andersen P, et al. Magnetic resonance studies of brain function and neurochemistry. *Annu Rev Biomed Eng*. 2000;2:633-660.
18. Kim SG, Ugurbil K. High-resolution functional magnetic resonance imaging of the animal brain. *Methods*. 2003;30:28-41.
19. Yacoub E, Duong TQ, Van De Moortele PF, et al. Spin-echo fMRI in humans using high spatial resolutions and high magnetic fields. *Magn Reson Med*. 2003;49:655-664.
20. Yacoub E, Van De Moortele PF, Shmuel A, Ugurbil K. Signal and noise characteristics of Hahn SE and GE BOLD fMRI at 7 T in humans. *Neuroimage*. 2005;24:738-750.
21. Vaughan JT, Garwood M, Collins CM, et al. 7T vs. 4T: RF power, homogeneity, and signal-to-noise comparison in head images. *Magn Reson Med*. 2001;46:24-30.
22. Duong TQ, Kim DS, Ugurbil K, Kim SG. Localized cerebral blood flow response at submillimeter columnar resolution. *Proc Natl Acad Sci U S A*. 2001;98:10904-10909.
23. Ugurbil K. Two decades of functional imaging: from nuclear spins to cortical columns. *Cognitive Critique*. 2012;4:121-186.
24. Ugurbil K. Imaging of brain function using deoxyhemoglobin and magnetic fields. In: Choi I-Y, Gruetter R, eds. *Neural Metabolism In Vivo*. New York, NY: Springer US; 2012:501-545.
25. Engel SA, Glover GH, Wandell BA. Retinotopic organization in human visual cortex and the spatial precision of functional MRI. *Cereb Cortex*. 1997;7:181-192.
26. Ronen I, Olman C, Kim SG, Ugurbil K, Toth LJ. Spatial relationship between neuronal activity and BOLD functional MRI. *Neuroimage*. 2004;21:876-885.
27. Park JC, Ronen I, Kim D-S, Ugurbil K. Spatial specificity of high resolution GE BOLD and CBF fMRI in the cat visual cortex. *Proc Intl Soc Mag Reson Med*. 2004;12:1014.
28. Park JC, Ronen I, Kim D-S, Ugurbil K. Spatial specificity of high resolution GE BOLD and Spin Ech (SE) BOLD fMRI in the cat visual cortex at 9.4 Tesla. *Proc Intl Soc Mag Reson Med*. 2005;13:31.
29. Olman CA, Harel N, Feinberg DA, et al. Layer-specific fMRI reflects different neuronal computations at different depths in human V1. *PLoS One*. 2012;7:e32536.
30. Zimmermann J, Goebel R, De Martino F, et al. Mapping the organization of axis of motion selective features in human area MT using high-field fMRI. *PLoS One*. 2011;6:e28716.
31. Polimeni JR, Fischl B, Greve DN, Wald LL. Laminar analysis of 7T BOLD using an imposed spatial activation pattern in human V1. *Neuroimage*. 2010;52:1334-1346.
32. Koopmans PJ, Barth M, Orzada S, Norris DG. Multi-echo fMRI of the cortical laminae in humans at 7 T. *Neuroimage*. 2011;56:1276-1285.
33. Yacoub E, Shmuel A, Logothetis N, Ugurbil K. Robust detection of ocular dominance columns in humans using Hahn Spin Echo BOLD functional MRI at 7 Tesla. *Neuroimage*. 2007;37:1161-1177.
34. Yacoub E, Harel N, Ugurbil K. High-field fMRI unveils orientation columns in humans. *Proc Natl Acad Sci U S A*. 2008;105:10607-10612.
35. Menon RS, Ogawa S, Strupp JP, Ugurbil K. Ocular dominance in human V1 demonstrated by functional magnetic resonance imaging. *J Neurophysiol*. 1997;77:2780-2787.
36. Cheng K, Waggoner RA, Tanaka K. Human ocular dominance columns as revealed by high-field functional magnetic resonance imaging. *Neuron*. 2001;32:359-374.
37. Goodyear BG, Menon RS. Brief visual stimulation allows mapping of ocular dominance in visual cortex using fMRI. *Hum Brain Mapp*. 2001;14:210-217.
38. Fukuda M, Moon CH, Wang P, Kim SG. Mapping iso-orientation columns by contrast agent-enhanced functional magnetic resonance imaging: reproducibility, specificity, and evaluation by optical imaging of intrinsic signal. *J Neurosci*. 2006;26:11821-11832.
39. Sun P, Ueno K, Waggoner RA, Gardner JL, Tanaka K, Cheng K. A temporal frequency-dependent functional architecture in human V1 revealed by high-resolution fMRI. *Nat Neurosci*. 2007;10:1404-1406.
40. Zhao F, Wang P, Hendrich K, Ugurbil K, Kim SG. Cortical layer-dependent BOLD and CBV responses measured by spin-echo and gradient-echo fMRI: insights into hemodynamic regulation. *Neuroimage*. 2006;30:1149-1160.
41. Zhao F, Wang P, Kim SG. Cortical depth-dependent gradient-echo and spin-echo BOLD fMRI at 9.4T. *Magn Reson Med*. 2004;51:518-524.
42. Kim SG, Duong TQ. Mapping cortical columnar structures using fMRI. *Physiol Behav*. 2002;77:641-644.
43. Duong TQ, Silva AC, Lee SP, Kim SG. Functional MRI of calcium-dependent synaptic activity: cross correlation with CBF and BOLD measurements. *Magn Reson Med*. 2000;43:383-392.
44. Harel N, Lin J, Moeller S, Ugurbil K, Yacoub E. Combined imaging-histological study of cortical laminar specificity of fMRI signals. *Neuroimage*. 2006;29:879-887.
45. Goense JB, Logothetis NK. Laminar specificity in monkey V1 using high-resolution SE-fMRI. *Magn Reson Imaging*. 2006;24:381-392.
46. Yu X, Glen D, Wang S, et al. Direct imaging of macrovascular and microvascular contributions to BOLD fMRI in layers IV-V of the rat whisker-barrel cortex. *Neuroimage*. 2012;59:1451-1460.
47. Mandeville JB, Marota JJ, Kosofsky BE, et al. Dynamic functional imaging of relative cerebral blood volume during rat forepaw stimulation. *Magn Reson Med*. 1998;39:615-624.
48. Smirnakis SM, Schmid MC, Weber B, Tolias AS, Augath M, Logothetis NK. Spatial specificity of BOLD versus cerebral blood volume fMRI for mapping cortical organization. *J Cereb Blood Flow Metab*. 2007;27:1248-1261.
49. Leite FP, Tsao D, Vanduffel W, et al. Repeated fMRI using iron oxide contrast agent in awake, behaving macaques at 3 Tesla. *Neuroimage*. 2002;16:283-294.
50. Logothetis NK, Pauls J, Augath M, Trinath T, Oeltermann A. Neurophysiological investigation of the basis of the fMRI signal. *Nature*. 2001;412:150-157.
51. Logothetis NK. What we can do and what we cannot do with fMRI. *Nature*. 2008;453:869-878.
52. Kim DS, Ronen I, Olman C, Kim SG, Ugurbil K, Toth LJ. Spatial relationship between neuronal activity and BOLD functional MRI. *Neuroimage*. 2004;21:876-885.
53. Leopold DA, Maier A. Ongoing physiological processes in the cerebral cortex. *Neuroimage*. 2012;62:2190-2200.
54. Scholvinck ML, Maier A, Ye FQ, Duyn JH, Leopold DA. Neural basis of global resting-state fMRI activity. *Proc Natl Acad Sci U S A*. 1 2010;107:10238-10243.
55. Shmuel A, Leopold DA. Neuronal correlates of spontaneous fluctuations in fMRI signals in monkey visual cortex: Implications for functional connectivity at rest. *Hum Brain Mapp*. 08;29:751-761.
56. Liu X, Zhu XH, Zhang Y, Chen W. Neural origin of spontaneous hemodynamic fluctuations in rats under burst-suppression anesthesia condition. *Cerebral Cortex*. 2011;21:374-384.
57. Biswal B, Yetkin FZ, Haughton VM, Hyde JS. Functional connectivity in the motor cortex of resting human brain using echo-planar MRI. *Magn Res Med*. 1995;34:537-541.
58. Fox MD, Raichle ME. Spontaneous fluctuations in brain activity observed with functional magnetic resonance imaging. *Nat Rev Neurosci*. 2007;8:700-711.
59. Vincent JL, Patel GH, Fox MD, et al. Intrinsic functional architecture in the anaesthetized monkey brain. *Nature*. 2007;447:83-86.

60. Beckmann CF, DeLuca M, Devlin JT, Smith SM. Investigations into resting-state connectivity using independent component analysis. *Philos Trans R Soc Lond B Biol Sci*. 2005;360:1001-1013.
61. Smith SM, Miller KL, Salimi-Khorshidi G, et al. Network modelling methods for FMRI. *Neuroimage*. 2011;54:875-891.
62. Smith SM, Beckmann CF, Andersson J, et al. Resting-state fMRI in the Human Connectome Project. *Neuroimage*. 2013;80:144-168.
63. Kim S-G, Hu X, Ugurbil K. Accurate T1 determination from inversion recovery images: application to human brain at 4 Tesla. *Magn Reson Med*. 1994;31:445-449.
64. Jezzard P, Duewell S, Balaban RS. MR relaxation times in human brain: measurement at 4 T. *Radiology*. 1996;199:773-779.
65. Bartha R, Michaeli S, Merkle H, et al. In vivo HO T(dagger) measurement in the human occipital lobe at 4T and 7T by Carr-Purcell MRI: detection of microscopic susceptibility contrast. *Magn Reson Med*. 02;47:742-750.
66. Michaeli S, Garwood M, Zhu XH, et al. Proton T relaxation study of water, N-acetylaspartate, and creatine in human brain using Hahn and Carr-Purcell spin echoes at 4T and 7T. *Magn Reson Med*. 2002;47:629-633.
67. Norris DG. High field human imaging. *J Magn Reson Imaging*. 2003;18:519-529.
68. Rooney W, Johnson G, Li X, et al. Magnetic field and tissue dependencies of human brain longitudinal 1H2O relaxation in vivo. *Magn Reson Med*. 2007;57:308-318.
69. Dobre MC, Marjanska M, Ugurbil K. Blood T1 measurement at high magnetic field strength. *Proc Intl Soc Mag Reson Med*. 2005;13:1162.
70. Bolan PJ, Yacoub E, Garwood M, Ugurbil K, Harel N. In vivo micro-MRI of intracortical neurovasculature. *NeuroImage*. 2006;32:62-69.
71. Duyn JH, van Gelderen P, Li TQ, de Zwart JA, Koretsky AP, Fukunaga M. High-field MRI of brain cortical substructure based on signal phase. *Proc Natl Acad Sci U S A*. 2007;104:11796-11801.
72. Marques JP, Maddage R, Mlynarik V, Gruetter R. On the origin of the MR image phase contrast: an in vivo MR microscopy study of the rat brain at 14.1T. *Neuroimage*. 2009;46:345-352.
73. Sati P, van Gelderen P, Silva AC, et al. Micro-compartment specific T2* relaxation in the brain. *Neuroimage*. 2013;77:268-278.
74. Lee J, Shmueli K, Kang BT, et al. The contribution of myelin to magnetic susceptibility-weighted contrasts in high-field MRI of the brain. *Neuroimage*. 2012;59:3967-3975.
75. Fukunaga M, Li TQ, van Gelderen P, et al. Layer-specific variation of iron content in cerebral cortex as a source of MRI contrast. *Proc Natl Acad Sci U S A*. 2010;107:3834-3839.
76. Li TQ, Yao B, van Gelderen P, et al. Characterization of T* heterogeneity in human brain white matter. *Magn Reson Med*. 2009;62:1652-1657.
77. Lodygensky GA, Marques JP, Maddage R, et al. In vivo assessment of myelination by phase imaging at high magnetic field. *Neuroimage*. 2012;59:1979-1987.
78. Jack CR, Jr, Garwood M, Wengenack TM, et al. In vivo visualization of Alzheimer's amyloid plaques by magnetic resonance imaging in transgenic mice without a contrast agent. *Magn Reson Med*. 2004;52:1263-1271.
79. Jack CR, Jr., Wengenack TM, Reyes DA, et al. In vivo magnetic resonance microimaging of individual amyloid plaques in Alzheimer's transgenic mice. *J Neurosci*. 2005;25:10041-10048.
80. Jenkins BG, Kraft E. Magnetic resonance spectroscopy in toxic encephalopathy and neurodegeneration. *Curr Opin Neurol*. 1999;12:753-760.
81. Choi IY, Lee SP, Guilfoyle DN, Helpern JA. In vivo NMR studies of neurodegenerative diseases in transgenic and rodent models. *Neurochem Res*. 2003;28:987-1001.
82. Michaelis T, Boretius S, Frahm J. Localized proton MRS of animal brain in vivo: models of human disorders. *Prog NMR Spect*. 2009;55:1-34.
83. Duarte JM, Lei H, Mlynarik V, Gruetter R. The neurochemical profile quantified by in vivo 1H NMR spectroscopy. *Neuroimage*. 2012;61:342-362.
84. Dautry C, Vaufrey F, Brouillet E, et al. Early N-acetylaspartate depletion is a marker of neuronal dysfunction in rats and primates chronically treated with the mitochondrial toxin 3- nitropropionic acid. *J Cereb Blood Flow Metab*. 2000;20:789-799.
85. Jenkins BG, Klivenyi P, Kustermann E, et al. Nonlinear decrease over time in N-acetyl aspartate levels in the absence of neuronal loss and increases in glutamine and glucose in transgenic Huntington's disease mice. *J Neurochem*. 2000;74:2108-2119.
86. Bossuet C, Vaufrey F, Conde F, et al. Up-regulation of glutamate concentration in the putamen and in the prefrontal cortex of asymptomatic SIVmac251-infected macaques without major brain involvement. *J Neurochem*. 2004;88:928-938.
87. Dedeoglu A, Choi JK, Cormier K, Kowall NW, Jenkins BG. Magnetic resonance spectroscopic analysis of Alzheimer's disease mouse brain that express mutant human APP shows altered neurochemical profile. *Brain Res*. 2004;1012:60-65.
88. Emir UE, Auerbach EJ, Moortele PF, et al. Regional neurochemical profiles in the human brain measured by H MRS at 7 T using local B shimming. *NMR Biomed*. 2012;25:152-160.
89. Tkac I, Oz G, Adriany G, Ugurbil K, Gruetter R. In vivo 1H NMR spectroscopy of the human brain at high magnetic fields: metabolite quantification at 4T vs. 7T. *Magn Reson Med*. 2009;62:868-879.
90. Pfeuffer J, Tkac I, Provencher SW, Gruetter R. Toward an in vivo neurochemical profile: quantification of 18 metabolites in short-echo-time H NMR spectra of the rat brain. *J Magn Reson*. 1999;141:104-120.
91. Tkac I, Henry PG, Andersen P, Keene CD, Low WC, Gruetter R. Highly resolved in vivo 1H NMR spectroscopy of the mouse brain at 9.4 T. *Magn Reson Med*. 2004;52:478-484.
92. Schwarcz A, Natt O, Watanabe T, Boretius S, Frahm J, Michaelis T. Localized proton MRS of cerebral metabolite profiles in different mouse strains. *Magn Reson Med*. 2003;49:822-827.
93. Holmay MJ, Terpstra M, Coles LD, et al. N-acetylcysteine boosts brain and blood glutathione in gaucher and Parkinson diseases. *Clin Neuropharmacol*. 2013;36:103-106.
94. Tkac I, Oz G. In vivo proton MR spectroscopy: animal and human applications at high fields. In: Garrido L, Beckmann N, eds. *New Applications of NMR in Drug Discovery and Development*. London, UK: Royal Society of Chemistry; 2013:237-258.
95. Bartha R, Drost DJ, Menon RS, Williamson PC. Comparison of the quantification precision of human short echo time H spectroscopy at 1.5 and 4.0 Tesla. *Magn Reson Med*. 2000;44:185-192.
96. Otazo R, Mueller B, Ugurbil K, Wald L, Posse S. Signal-to-noise ratio and spectral linewidth improvements between 1.5 and 7 Tesla in proton echo-planar spectroscopic imaging. *Magn Reson Med*. 2006;56:1200-1210.
97. Mekle R, Mlynarik V, Gambarota G, Hergt M, Krueger G, Gruetter R. MR spectroscopy of the human brain with enhanced signal intensity at ultrashort echo times on a clinical platform at 3T and 7T. *Magn Reson Med*. 2009;61:1279-1285.
98. Clark JB. N-acetyl aspartate: a marker for neuronal loss or mitochondrial dysfunction. *Dev Neurosci*. 1998;20:271-276.
99. Demougeot C, Garnier P, Mossiat C, et al. N-Acetylaspartate, a marker of both cellular dysfunction and neuronal loss: its relevance to studies of acute brain injury. *J Neurochem*. 2001;77:408-415.
100. Petroff OA, Pleban LA, Spencer DD. Symbiosis between in vivo and in vitro NMR spectroscopy: the creatine, N-acetylaspartate, glutamate, and GABA content of the epileptic human brain. *Magn Reson Imaging*. 1995;13:1197-1211.
101. Storm-Mathisen J, Danbolt NC, Rothe F, et al. Ultrastructural immunocytochemical observations on the localization, metabolism and transport of glutamate in normal and ischemic brain tissue. *Prog Brain Res*. 1992;94:225-241.
102. Oz G, Tkac I, Charnas LR, et al. Assessment of adrenoleukodystrophy lesions by high field MRS in non-sedated pediatric patients. *Neurology*. 2005;64:434-441.
103. Marjanska M, Curran GL, Wengenack TM, et al. Monitoring disease progression in transgenic mouse models of Alzheimer's disease with proton magnetic resonance spectroscopy. *Proc Natl Acad Sci U S A*. 2005;102:11906-11910.
104. Andreassen OA, Jenkins BG, Dedeoglu A, et al. Increases in cortical glutamate concentrations in transgenic amyotrophic lateral sclerosis mice are attenuated by creatine supplementation. *J Neurochem*. 2001;77:383-390.
105. Ottersen OP, Storm-Mathisen J. Glutamate- and GABA-containing neurons in the mouse and rat brain, as demonstrated with a new immunocytochemical technique. *J Comp Neurol*. 1984;229:374-392.
106. Palmi M, Brooke S, Smith AD, Bolam JP. GABA-like immunoreactivity in different cellular populations of cerebellar cortex of rats before and after treatment with amino-oxyacetic acid. *Brain Res*. 1991;543:277-286.

107. Brand A, Richter-Landsberg C, Leibfritz D. Multinuclear NMR studies on the energy metabolism of glial and neuronal cells. *Dev Neurosci*. 1993;15:289-298.
108. Schuhmann MU, Stiller D, Skardelly M, et al. Metabolic changes in the vicinity of brain contusions: a proton magnetic resonance spectroscopy and histology study. *J Neurotrauma*. 2003;20:725-743.
109. Pouwels PJ, Kruse B, Korenke GC, Mao X, Hanefeld FA, Frahm J. Quantitative proton magnetic resonance spectroscopy of childhood adrenoleukodystrophy. *Neuropediatrics*. 1998;29:254-264.
110. Kantarci K, Petersen RC, Boeve BF, et al. 1H MR spectroscopy in common dementias. *Neurology*. 2004;63:1393-1398.
111. Vrenken H, Barkhof F, Uitdehaag BM, Castelijns JA, Polman CH, Pouwels PJ. MR spectroscopic evidence for glial increase but not for neuro-axonal damage in MS normal-appearing white matter. *Magn Reson Med*. 2005;53:256-266.
112. Fisher SK, Novak JE, Agranoff BW. Inositol and higher inositol phosphates in neural tissues: homeostasis, metabolism and functional significance. *J Neurochem*. 2002;82:736-754.
113. Kim JP, Lentz MR, Westmoreland SV, et al. Relationships between astrogliosis and 1H MR spectroscopic measures of brain choline/creatine and myo-inositol/creatine in a primate model. *Am J Neuroradiol*. 2005;26:752-759.
114. Urenjak J, Williams SR, Gadian DG, Noble M. Proton nuclear magnetic resonance spectroscopy unambiguously identifies different neural cell types. *J Neurosci*. 1993;13:981-989.
115. Bitsch A, Bruhn H, Vougioukas V, et al. Inflammatory CNS demyelination: histopathologic correlation with in vivo quantitative proton MR spectroscopy. *Am J Neuroradiol*. 1999;20:1619-1627.
116. Mountford CE, Stanwell P, Lin A, Ramadan S, Ross B. Neurospectroscopy: the past, present and future. *Chem Rev*. 2010;110:3060-3086.
117. Zacharoff L, Tkac I, Song Q, et al. Cortical metabolites as biomarkers in the R6/2 model of Huntington's disease. *J Cereb Blood Flow Metab*. 2012;32:502-514.
118. Tkac I, Henry PG, Zacharoff L, et al. Homeostatic adaptations in brain energy metabolism in mouse models of Huntington disease. *J Cereb Blood Flow Metab*. 2012;32:1977-1988.
119. Terpstra M, Marjanska M, Henry PG, Tkac I, Gruetter R. Detection of an antioxidant profile in the human brain in vivo via double editing with MEGA-PRESS. *Magn Reson Med*. 2006;56:1192-1199.
120. Tkac I, Rao R, Georgieff MK, Gruetter R. Developmental and regional changes in the neurochemical profile of the rat brain determined by in vivo 1H NMR spectroscopy. *Magn Reson Med*. 2003;50:24-32.
121. Valette J, Guillermier M, Besret L, Hantraye P, Bloch G, Lebon V. Isoflurane strongly affects the diffusion of intracellular metabolites, as shown by 1H nuclear magnetic resonance spectroscopy of the monkey brain. *J Cereb Blood Flow Metab*. 2007;27:588-596.
122. Lei H, Duarte JM, Mlynarik V, Python A, Gruetter R. Deep thiopental anesthesia alters steady-state glucose homeostasis but not the neurochemical profile of rat cortex. *J Neurosci Res*. 2010;88:413–419.
123. Baker M. In biomarkers we trust? *Nat Biotechnol*. 05;23:297-304.
124. Mlynarik V, Cacquevel M, Sun-Reimer L, et al. Proton and phosphorus magnetic resonance spectroscopy of a mouse model of Alzheimer's disease. *J Alzheimers Dis*. 2012;31(suppl 3):S87-S99.
125. Chassain C, Bielicki G, Keller C, Renou JP, Durif F. Metabolic changes detected in vivo by 1H MRS in the MPTP-intoxicated mouse. *NMR Biomed*. 10;23:547-553.
126. Emir UE, Tuite PJ, Oz G. Elevated pontine and putamenal GABA levels in mild-moderate Parkinson disease detected by 7 tesla proton MRS. *PLoS One*. 2012;7:e30918.
127. Heikkinen T, Lehtimaki K, Vartiainen N, et al. Characterization of neurophysiological and behavioral changes, MRI brain volumetry and 1H MRS in zQ175 knock-in mouse model of Huntington's disease. *PLoS One*. 2012;7:e50717.
128. Tkac I, Zacharoff L, Dubinsky JM. Longitudinal changes in neurochemical profiles of Huntington's disease mouse models. Paper presented at: 20th Scientific Meeting of the ISMRM; May 5-11, 2012; Melbourne, Australia.
129. Unschuld PG, Edden RA, Carass A, et al. Brain metabolite alterations and cognitive dysfunction in early Huntington's disease. *Mov Disord*. 2012;27:895-902.
130. van den Bogaard SJ, Dumas EM, Teeuwisse WM, et al. Exploratory 7-Tesla magnetic resonance spectroscopy in Huntington's disease provides in vivo evidence for impaired energy metabolism. *J Neurol*. 2011;258:2230-2259.
131. DeKosky ST, Marek K. Looking backward to move forward: early detection of neurodegenerative disorders. *Science*. 2003;302:830-834.
132. Burright EN, Clark HB, Servadio A, et al. SCA1 transgenic mice: a model for neurodegeneration caused by an expanded CAG trinucleotide repeat. *Cell*. 1995;82:937-948.
133. Oz G, Nelson CD, Koski DM, et al. Noninvasive detection of presymptomatic and progressive neurodegeneration in a mouse model of spinocerebellar ataxia type 1. *J Neurosci*. 2010;30:3831-3838.
134. Oz G, Hutter D, Tkac I, et al. Neurochemical alterations in spinocerebellar ataxia type 1 and their correlations with clinical status. *Mov Disord*. 2010;25:1253-1261.
135. Choi JK, Jenkins BG, Carreras I, et al. Anti-inflammatory treatment in AD mice protects against neuronal pathology. *Exp Neurol*. 2010;223:377-384.
136. Oz G, Vollmers ML, Nelson CD, et al. In vivo monitoring of recovery from neurodegeneration in conditional transgenic SCA1 mice. *Exp Neurol*. 2011;232:290-298.
137. Iltis I, Koski DM, Eberly LE, et al. Neurochemical changes in the rat prefrontal cortex following acute phencyclidine treatment: an in vivo localized H MRS study. *NMR Biomed*. 2009;22:737-744.
138. de Graaf RA, Patel AB, Rothman DL, Behar KL. Acute regulation of steady-state GABA levels following GABA-transaminase inhibition in rat cerebral cortex. *Neurochem Int*. 2006;48:508-514.
139. Petroff OA, Hyder F, Collins T, Mattson RH, Rothman DL. Acute effects of vigabatrin on brain GABA and homocarnosine in patients with complex partial seizures. *Epilepsia*. 1999;40:958-964.
140. Zhu XH, Merkle H, Kwag JH, Ugurbil K, Chen W. 17O relaxation time and NMR sensitivity of cerebral water and their field dependence. *Magn Reson Med*. 2001;45:543-549.
141. Hoult DI, Richards RE. The signal-to-noise ratio of the nuclear magnetic resonance phenomenon. *J Magn Reson*. 1976;24:71-85.
142. Zhu XH, Zhang Y, Tian RX, et al. Development of O NMR approach for fast imaging of cerebral metabolic rate of oxygen in rat brain at high field. *Proc Natl Acad Sci U S A*. 2002;99:13194-13199.
143. Zhang N, Zhu XH, Lei H, Ugurbil K, Chen W. Simplified methods for calculating cerebral metabolic rate of oxygen based on 17O magnetic resonance spectroscopic imaging measurement during a short 17O2 inhalation. *J Cereb Blood Flow Metab*. 2004;24:840-848.
144. Zhu XH, Zhang N, Zhang Y, Zhang X, Ugurbil K, Chen W. In vivo O NMR approaches for brain study at high field. *NMR Biomed*. 2005;18:83-103.
145. Zhu XH, Zhang N, Zhang Y, Ugurbil K, Chen W. New insights into central roles of cerebral oxygen metabolism in the resting and stimulus-evoked brain. *J Cereb Blood Flow Metab*. 2009;29:10-18.
146. Gruetter R, Seaquist ER, Ugurbil K. A mathematical model of compartmentalized neurotransmitter metabolism in the human brain. *Am J Physiol Endocrinol Metab*. 2001;281:E100-112.
147. Oz G, Berkich DA, Henry PG, et al. Neuroglial metabolism in the awake rat brain: CO2 fixation increases with brain activity. *J Neurosci*. 2004;24:11273-11279.
148. Choi IY, Gruetter R. In vivo 13C NMR assessment of brain glycogen concentration and turnover in the awake rat. *Neurochem Int*. 2003;43:317-322.
149. Choi IY, Seaquist ER, Gruetter R. Effect of hypoglycemia on brain glycogen metabolism in vivo. *J Neurosci Res*. 2003;72:25-32.
150. Gruetter R. Glycogen: the forgotten cerebral energy store. *J Neurosci Res*. 2003;74:179-183.
151. Gruetter R, Adriany G, Choi IY, Henry PG, Lei H, Oz G. Localized in vivo 13C NMR spectroscopy of the brain. *NMR Biomed*. 2003;16:313-338.
152. Oz G, Henry PG, Seaquist ER, Gruetter R. Direct, noninvasive measurement of brain glycogen metabolism in humans. *Neurochem Int*. 2003;43:323-329.
153. Seaquist ER, Damberg GS, Tkac I, Gruetter R. The effect of insulin on in vivo cerebral glucose concentrations and rates of glucose transport/metabolism in humans. *Diabetes*. 2001;50:2203-2209.
154. Choi IY, Lee SP, Kim SG, Gruetter R. In vivo measurements of brain glucose transport using the reversible Michaelis-Menten model and simultaneous measurements of cerebral blood flow changes during hypoglycemia. *J Cereb Blood Flow Metab*. 2001;21:653-663.

155. Chen W, Zhu XH, Gruetter R, Seaquist ER, Adriany G, Ugurbil K. Study of tricarboxylic acid cycle flux changes in human visual cortex during hemifield visual stimulation using H-{C} MRS and fMRI. *Magn Reson Med*. 2001;45:349-355.
156. Gruetter R, Ugurbil K, Seaquist ER. Steady-state cerebral glucose concentrations and transport in the human brain. *J Neurochem*. 1998;70:397-408.
157. Lei H, Ugurbil K, Chen W. Measurement of unidirectional Pi to ATP flux in human visual cortex at 7 T by using in vivo 31P magnetic resonance spectroscopy. *Proc Natl Acad Sci U S A*. 2003;100:14409-14414.
158. Oz G, Tesfaye N, Kumar A, Deelchand DK, Eberly LE, Seaquist ER. Brain glycogen content and metabolism in subjects with type 1 diabetes and hypoglycemia unawareness. *J Cereb Blood Flow Metab*. 2012;32:256-263.
159. Hattingen E, Magerkurth J, Pilatus U, et al. Phosphorus and proton magnetic resonance spectroscopy demonstrates mitochondrial dysfunction in early and advanced Parkinson's disease. *Brain*. 2009;132(Pt 12):3285-3297.
160. Oz G. MR Spectroscopy in health and disease. In: Manto M, Gruol DL, Schmahmann JD, Koibuchi N, Rossi F, eds. *Handbook of the Cerebellum and Cerebellar Disorders*. Vol 1. New York, NY: Springer Dordrecht; 2013:713-733.